

RESEARCH LETTER

10.1002/2017GL073155

Key Points:

- Coupled dynamical prediction system skillfully predicts regional sea ice extent on seasonal timescales
- Ocean subsurface temperature initialization yields North Atlantic regional winter skill at lead times of 5–11 months
- Sea ice thickness initialization provides a key source of summer regional skill at lead times of 1–4 months

Supporting Information:

- Supporting Information S1

Correspondence to:

M. Bushuk
mitchell.bushuk@noaa.gov

Citation:

Bushuk, M., R. Msadek, M. Winton, G. A. Vecchi, R. Gudgel, A. Rosati, and X. Yang (2017), Skillful regional prediction of Arctic sea ice on seasonal timescales, *Geophys. Res. Lett.*, *44*, 4953–4964, doi:10.1002/2017GL073155.

Received 19 FEB 2017

Accepted 25 APR 2017

Accepted article online 27 APR 2017

Published online 21 MAY 2017

Skillful regional prediction of Arctic sea ice on seasonal timescales

Mitchell Bushuk¹ , Rym Msadek², Michael Winton³, Gabriel A. Vecchi^{1,4} , Rich Gudgel³, Anthony Rosati³, and Xiaosong Yang³

¹Atmospheric and Oceanic Sciences Program, Princeton University, Princeton, New Jersey, USA, ²CNRS/CERFACS, CECI UMR 5318, Toulouse, France, ³National Oceanic and Atmospheric Administration/Geophysical Fluid Dynamics Laboratory, Princeton University, Princeton, New Jersey, USA, ⁴Department of Geosciences, Princeton University, Princeton, New Jersey, USA

Abstract Recent Arctic sea ice seasonal prediction efforts and forecast skill assessments have primarily focused on pan-Arctic sea ice extent (SIE). In this work, we move toward stakeholder-relevant spatial scales, investigating the regional forecast skill of Arctic sea ice in a Geophysical Fluid Dynamics Laboratory (GFDL) seasonal prediction system. Using a suite of retrospective initialized forecasts spanning 1981–2015 made with a coupled atmosphere-ocean-sea ice-land model, we show that predictions of detrended regional SIE are skillful at lead times up to 11 months. Regional prediction skill is highly region and target month dependent and generically exceeds the skill of an anomaly persistence forecast. We show for the first time that initializing the ocean subsurface in a seasonal prediction system can yield significant regional skill for winter SIE. Similarly, as suggested by previous work, we find that sea ice thickness initial conditions provide a crucial source of skill for regional summer SIE.

1. Introduction

Arctic sea ice has undergone rapid changes over the satellite era, characterized by a decline in pan-Arctic September sea ice extent (SIE) of roughly –14% per decade [Serreze *et al.*, 2007; Cavalieri and Parkinson, 2012; Stroeve *et al.*, 2014a], substantial thinning [Rothrock *et al.*, 1999; Kwok and Rothrock, 2009], a transition from multiyear to first-year ice [Rigor and Wallace, 2004; Maslanik *et al.*, 2011], and longer melt seasons [Perovich and Polashenski, 2012; Stroeve *et al.*, 2014a]. These striking changes and their implications for stakeholders have sparked research interest in the seasonal prediction and predictability of Arctic sea ice. Seasonal prediction skill for detrended pan-Arctic SIE has been assessed in a number of global climate model (GCM)-based forecast systems. These studies, based on suites of initialized retrospective forecasts (hindcasts), report significant forecast skill relative to the linear trend at lead times of 1–6 months, depending on the target month and model used [Wang *et al.*, 2013; Chevallier *et al.*, 2013; Sigmond *et al.*, 2013; Merryfield *et al.*, 2013; Msadek *et al.*, 2014; Peterson *et al.*, 2015; Blanchard-Wrigglesworth *et al.*, 2015; Guemas *et al.*, 2016]. Statistical forecast methods have also been shown to skillfully predict detrended pan-Arctic SIE at lead times up to 6 months [Lindsay *et al.*, 2008; Stroeve *et al.*, 2014b; Schröder *et al.*, 2014; Wang *et al.*, 2016; Yuan *et al.*, 2016; Petty *et al.*, 2017].

In parallel with the development of these quasi-operational dynamical prediction systems, a number of “perfect model” studies, which examine how well a model can predict itself, have been performed to quantify upper bounds for the forecast skill achievable in such systems. These perfect model studies have shown that pan-Arctic SIE is potentially predictable at 12–24 month lead times, substantially longer than the current skill of GCM-based prediction systems [Koenigk and Mikolajewicz, 2009; Holland *et al.*, 2011; Blanchard-Wrigglesworth *et al.*, 2011a; Tietsche *et al.*, 2014; Germe *et al.*, 2014]. Analogous to the so-called quiet revolution in numerical weather prediction [Bauer *et al.*, 2015], closing this prediction skill gap will require improvements in both model physics and initial conditions (ICs).

These studies have defined baselines for the current and potential seasonal forecast skill of pan-Arctic SIE. While this body of work represents a crucial first step, its utility is somewhat limited for stakeholders, who are primarily interested in sea ice predictions on regional and sub-regional spatial scales. Regional sea ice predictions are a pressing need for a broad stakeholder group, including northern communities [Ford and Smit, 2004], wildlife [Regehr *et al.*, 2007], shipping industries [Smith and Stephenson, 2013; Melia *et al.*, 2016];

Pizzolato et al., 2016; Laliberté et al., 2016], fisheries [*Wyllie-Echeverria and Wooster, 1998*], and natural resource industries [*Jung et al., 2016*]. The decline of regional SIE is ubiquitous in the Arctic, with statistically significant negative SIE trends in all regions except for the Bering Sea, which has a small positive trend that is not statistically significant [*Cavalieri and Parkinson, 2012*].

Baselines for current and potential regional Arctic SIE prediction skill in dynamical forecast systems have yet to be thoroughly established. The study of *Sigmond et al. [2016]* demonstrated skillful predictions of detrended regional ice advance and retreat dates, with notably high skill for advance dates in Hudson Bay, Baffin Bay/Labrador Sea, and the Chukchi Sea. *Krikken et al. [2016]* investigated detrended regional sea ice area predictions (using three initialization months) and found skillful forecasts up to 6 month lead times for the Barents/Kara Seas and the Northeast passage region. The work of *Day et al. [2014a]* identified the seasonal ice zones of the North Atlantic sector as the regions with highest potential SIE predictability (at lead times of 1.5–2.5 years). *Yeager et al. [2015]* additionally demonstrated skillful predictions of decadal SIE trends in this sector, which they attributed to predictable variations in the Atlantic thermohaline circulation.

In this work, we present the first comprehensive assessment of regional Arctic SIE prediction skill within a coupled dynamical prediction system. Using a suite of retrospective seasonal forecasts, we examine regional SIE skill in fourteen Arctic regions for all target months and lead times of 0–11 months. We study the physical mechanisms underlying this regional skill, identifying critical roles for initialization of subsurface ocean temperature and sea ice thickness in regional predictions of winter and summer SIE, respectively. Finally, implications for future dynamical prediction systems are discussed.

2. Methods

2.1. The GFDL Prediction System

This study is based on a suite of retrospective seasonal forecasts spanning 1981–2015 made with one of the Geophysical Fluid Dynamics Laboratory (GFDL) prediction systems. The prediction system consists of a fully coupled atmosphere-land-sea ice-ocean GCM with initial conditions (ICs) from a coupled data assimilation system. The forecast model is the GFDL Forecast-oriented Low Ocean Resolution (FLOR) [*Vecchi et al., 2014*] model, which employs a relatively high horizontal resolution of 0.5° in the atmosphere and land components, and 1° resolution in the ocean and sea ice components. The sea ice model of FLOR is the Sea Ice Simulator version 1 (SIS1) [*Delworth et al., 2006*]. This model uses an elastic-viscous-plastic rheology for the calculation of internal ice forces [*Hunke and Dukowicz, 1997*], an ice-thickness distribution with five thickness categories [*Bitz et al., 2001*], and a three-layer thermodynamic formulation with one snow layer and two ice layers [*Winton, 2000*]. The FLOR prediction system exhibits seasonal forecast skill for a diverse set of climate applications, including tropical cyclone activity [*Vecchi et al., 2014*], pan-Arctic SIE [*Msadek et al., 2014*], surface-air temperature and precipitation over land [*Jia et al., 2015*], and regional sea surface temperature (SST) [*Stock et al., 2015*].

The seasonal forecasts are initialized using an Ensemble Kalman Filter-coupled Data Assimilation system (ECDA) [*Zhang et al., 2007*]. The ECDA system assimilates subsurface ocean temperature and salinity data, satellite SST, and atmospheric reanalysis data from National Centers for Environmental Prediction. The subsurface ocean data comes from the World Ocean Database [*Levitus et al., 2013*], the Global Temperature and Salinity Profile Programme [*Sun et al., 2010*], and the Argo Program [*Roemmich et al., 2004*]. These data sources comprise a wide variety of historical oceanic observations including expendable bathythermograph data, conductivity-temperature-depth data, moored buoy data, mechanical bathythermograph data, ocean station data (or so-called bottle data), and autonomous ocean profiles (since the introduction of Argo floats in 2000). Note that ECDA does not directly assimilate any sea ice concentration (SIC) or thickness (SIT) data. The ocean and sea ice ICs are taken directly from ECDA, whereas the atmosphere and land ICs are produced via a suite of “Atmospheric Model Intercomparison Project-style” atmosphere-land only simulations forced by observed SST and sea ice. This technique is used to initialize the atmosphere and land components because FLOR employs a higher resolution in these components than ECDA, which was built on the CM2.1 model [*Delworth et al., 2006*]. The ensemble forecast experiments are initialized with a 12-member ensemble on the first of each month from January 1981 to December 2015 and run for 1 year. This suite of hindcasts allows us to assess the skill of this forecast system against nearly all of the available satellite SIC record, which begins in November 1978.

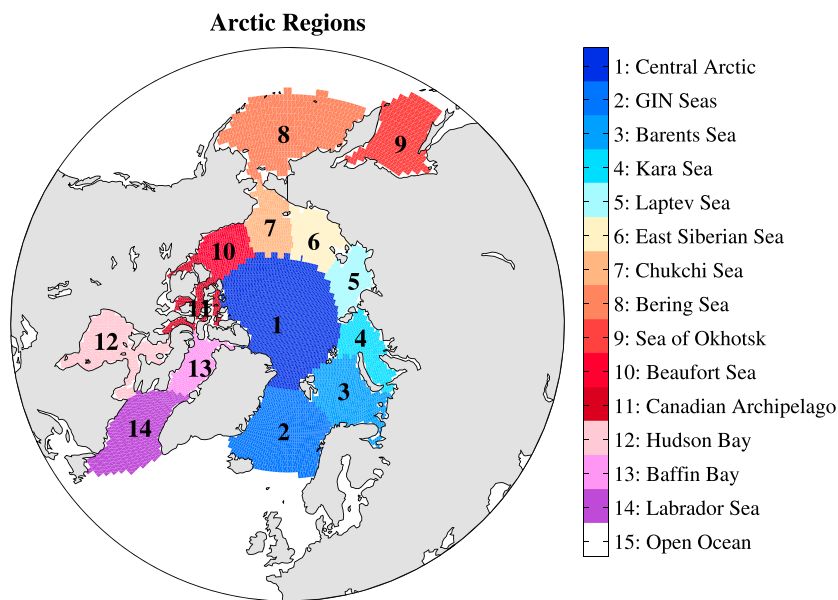


Figure 1. The Arctic regions considered in this study.

2.2. Forecast Skill Assessment

In this study, we assess the ability of the FLOR prediction system to predict regional SIE in the 14 Arctic regions shown in Figure 1. The regional domains are chosen following the Day *et al.* [2014a] definitions. We compute prediction skill scores for each region, target months from January to December, and lead times from 0 to 11 months. “Target month” refers to the month that we are trying to predict, and “lead time” refers to the number of months prior to the target month that the forecast was initialized. We verify our predictions against passive microwave satellite SIC observations from the National Snow and Ice Data Center (NSIDC). We use monthly averaged SIC data processed using the NASA team algorithm [Cavalieri *et al.*, 1996], and regrid these data from the native NSIDC 25 km polar stereographic grid onto the 1° GFDL sea ice grid. The regridding was performed to avoid systematic SIE biases associated with the different land-sea masks of the two grids.

We assess prediction skill via the anomaly correlation coefficient (ACC). The ACC is the Pearson correlation coefficient between the predicted and observed regional SIE time series. The predicted regional SIE is computed in two steps: (1) we compute the ensemble-mean predicted SIC and (2) we compute an areal sum of all grid points in the region of interest with SIC $\geq 15\%$. In order to focus on skill relative to the long-term trend, we remove a linear trend forecast from the observed and predicted SIE time series before computing ACC values. The linear trend forecast is computed using only past data and is updated each year. For the first three hindcast years (1982–1984), we assume a linear trend of zero. We test whether the ACC values are significantly greater than 0 using a *t* test with a confidence level of 95%. The effective number of degrees of freedom for the *t* test is given by $N^* = \frac{1-r_1r_2}{1+r_1r_2} N$, where $N = 34$ is the number of years in the time series, and r_1 and r_2 are the lag-1 year autocorrelation values for each time series [Bretherton *et al.*, 1999]. Using this approach, we compute significance thresholds for each region, target month, and lead time. These thresholds vary regionally between 0.29 and 0.38.

We compare our prediction skill to an anomaly persistence forecast, which is the forecast obtained by persisting the observed anomaly of the initial month up to the target month. The anomalies in the persistence forecast may be defined relative to either the long-term climatology or the long-term linear trend, depending on whether one is assessing skill for total anomalies or detrended anomalies, respectively. We also compared our prediction skill to a damped anomaly persistence forecast [Van den Dool, 2006]. In terms of ACC, anomaly persistence is slightly more skillful than damped anomaly persistence, which motivated its use as the baseline forecast in this study.

3. Results

3.1. Arctic Regional Prediction Skill

In Figure 2, we plot the GFDL-FLOR Arctic regional prediction skill for detrended SIE. The prediction skill for total anomalies (nondetrended) is higher in all regions (see Figure S1 in the supporting information), due to predictability from negative regional SIE trends and the ability of the forecast system to capture these trends [Msadek *et al.*, 2014]. The detrended regional SIE forecast skill in Figure 2 generically exceeds that of a persistence forecast (see triangles in Figure 2). This indicates that there are dynamical sources of predictability beyond SIE anomaly persistence which this prediction system is able to capture. Interestingly, each Arctic region displays a unique correlation structure. These correlation structures are the result of three interrelated factors: (1) the inherent predictability of SIE in each region; (2) the accuracy of the forecast ICs; and (3) the ability of the model to dynamically evolve the IC fields and simulate regional SIE. Below, we highlight some key features of the regional SIE predictions.

Regional prediction skill is notably high for winter predictions of SIE in the North Atlantic sector. The Barents and Greenland-Iceland-Norwegian (GIN) Seas have statistically significant skill at lead times ranging from 5 to 9 months for target months of December–March (time series of January Barents SIE predictions are shown in Figure S2). Labrador Sea skill is the highest of any region, with significant skill beyond 7 months for target months of December–July. These skillful long-lead regional winter predictions correspond to forecasts initialized the previous summer and spring, often in months with little sea ice cover. Ahead in section 3.2, we investigate the sources of skill for these winter SIE predictions. In contrast to the North Atlantic sector, the seasonal ice zones of the North Pacific sector (the Bering Sea and Sea of Okhotsk) display little prediction skill beyond 3 month lead times.

The prediction system also displays significant summer SIE skill in the East Siberian, Laptev, Chukchi, and Beaufort Seas (time series of September East Siberian SIE predictions are shown in Figure S2). The summer SIE predictions in these regions are skillful at lead times of 1–4 months, lacking the long-lead skill of the winter North Atlantic predictions. The East Siberian, Laptev, and Beaufort Seas each display a barrier of prediction skill, in which skill drops off sharply in a certain initialization month. For the East Siberian and Laptev seas, this skill barrier corresponds to forecasts initialized before May, whereas for the Beaufort Sea, the barrier corresponds to forecasts initialized before June. These skill barriers can be identified in the ACC plots as diagonal lines corresponding to initial months May and June, respectively. A similar predictability barrier has been identified in the work of Day *et al.* [2014a], which showed that perfect model forecasts initialized in May lose skill more rapidly than forecasts initialized in July. The predictions also have skill for summer SIE in the Canadian Archipelago; however, this result should be viewed cautiously given the coarse model grid and relatively small number of grid points in this region. We further investigate the sources of summer SIE prediction skill in section 3.3, ahead.

In addition to skillfully predicting regional SIE minima and maxima, the forecasts also have skill in predicting melt season (June–July–August) and growth season (November–December) anomalies in Hudson Bay at lead times of 3–11 months. Forecast skill in Baffin Bay, another region that rapidly transitions from being ice covered to ice free, is substantially lower.

Pan-Arctic SIE represents the sum total of these diverse regional contributions. The FLOR prediction system generally has skill in predicting detrended pan-Arctic SIE at lead times of 1–5 months [Msadek *et al.*, 2014]. The month of June is a clear exception to this, with low skill even for lead-0 predictions. The pan-Arctic correlation structure displays two “lobes” of skill which peak in April and October, following the SIE maximum and minimum, respectively (Figure 2, top left panel). Skill drops rapidly in the months of June and December, which are the months when the ice edge transitions between the Central Arctic and the seasonal ice zones. The persistence forecast also displays a similar two-lobe correlation structure (see Figure S3), with low skill in June, July, November, and December, indicating that the FLOR ACC structure is related to the inherent persistence of pan-Arctic SIE anomalies. A similar link between persistence and predictability was found in the perfect model study of Day *et al.* [2014a]. Note that FLOR's low June prediction skill is not a generic feature of other dynamical prediction systems (compare Figure 5b of Wang *et al.* [2013], Figure 1ab of Merryfield *et al.* [2013], Figure 3b of Sigmond *et al.* [2013], and Figure 8a of Peterson *et al.* [2015]); however, a similar decrease in skill between September/October and November/December is seen in some systems [Wang *et al.*, 2013; Merryfield *et al.*, 2013; Sigmond *et al.*, 2013].

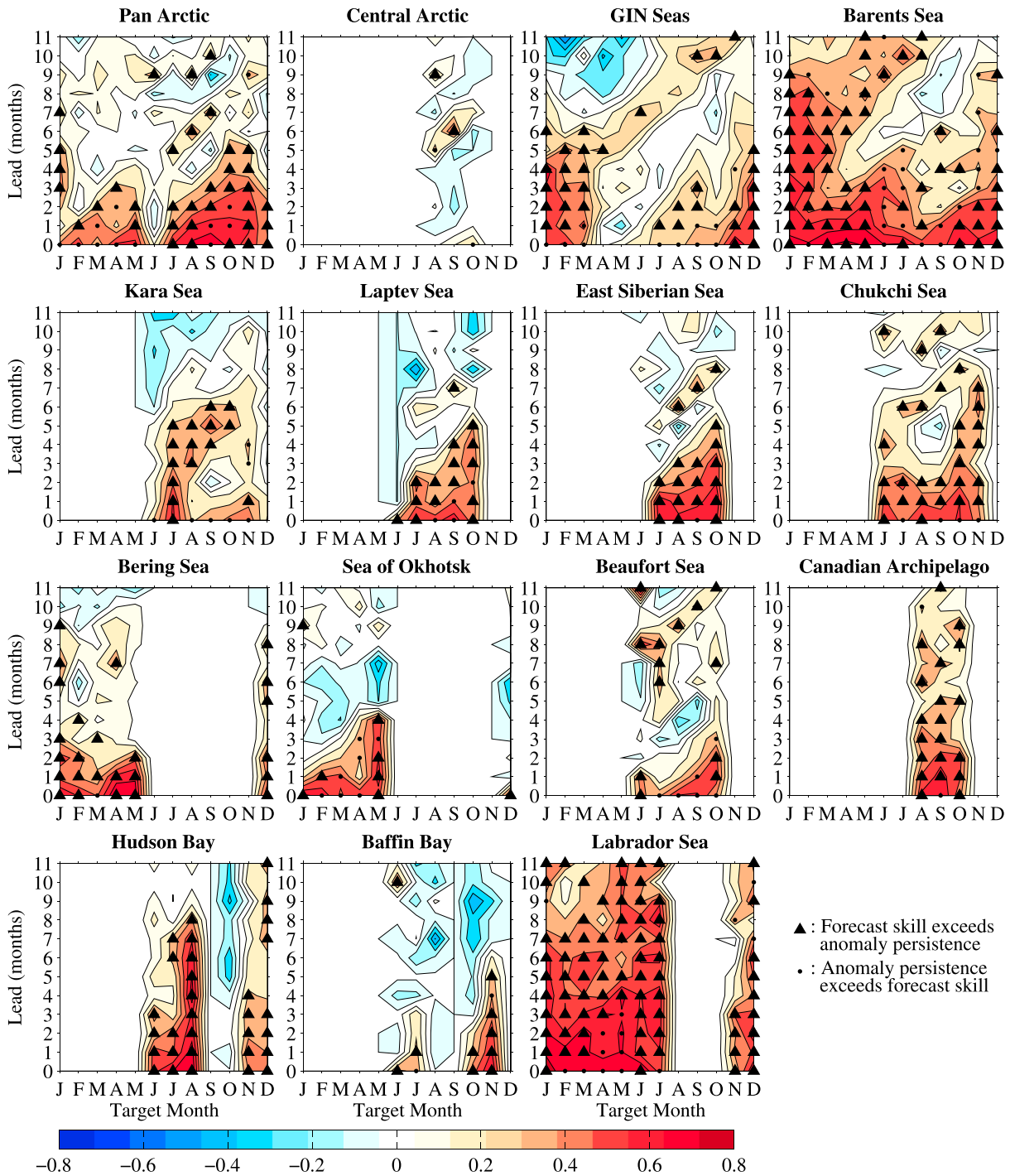


Figure 2. Seasonal prediction skill (ACC) for detrended regional Arctic SIE. The triangle and dot markers indicate months in which the ACC values are statistically significant at the 95% confidence level. Triangles indicate months in which the dynamical model's skill exceeds that of a persistence forecast, and circles indicate months in which the persistence forecast exceeds the model's skill. Correlations are only plotted for target months with SIE standard deviation greater than $0.03 \times 10^6 \text{ km}^2$.

We also assessed regional prediction skill for detrended SIE using a mean squared skill score (MSSS) metric [Murphy, 1988; Lindsay *et al.*, 2008]. The regional skill differences in MSSS are broadly consistent with the ACC results, showing highest skill in the North Atlantic sector and lower skill in the North Pacific and summer sea ice regions (see Figure S4).

3.2. Sources of Winter Regional Skill: Ocean Temperature Initialization

Next, we consider the physical mechanisms underlying the long-lead regional prediction skill for North Atlantic winter SIE. We first note that SIE anomalies in the Barents, Labrador, and GIN Seas are more persistent than anomalies in the Bering Sea and Sea of Okhotsk (see Figure S3). This additional persistence contributes to the superior skill of North Atlantic SIE forecasts relative to their North Pacific counterparts. A key difference between the FLOR predictions and the persistence forecasts is that the FLOR predictions remain skillful over the summer initialization months, while persistence does not (compare Figures 2 and S3 for the Barents, GIN, and Labrador Seas). These summer initialization months have little sea ice coverage and, therefore, require another source of memory to provide winter SIE prediction skill. On these 4–11 month timescales, persistent anomalies in upper ocean heat content represent a candidate source for this memory. Indeed, earlier work has shown that summer SST anomalies provide an important source of predictability for SIE anomalies in the ice growth season [Blanchard-Wrigglesworth *et al.*, 2011b; Day *et al.*, 2014a; Bushuk *et al.*, 2014, 2015; Bushuk and Giannakis, 2015; Sigmond *et al.*, 2016; Cheng *et al.*, 2016; Bushuk and Giannakis, 2017]. In order to exploit the intrinsic memory of the ocean, the forecast system must be able to initialize and dynamically evolve ocean properties through the ice-free summer months and into the ice growth season. To investigate this in the FLOR prediction system, we ask the following: Is there a relation between winter regional SIE and earlier ocean temperature ICs?

In Figure 3 we plot correlation values, as a function of ocean depth and forecast lead time, between observed regional SIE and earlier regional-mean ocean temperature ICs. We focus on the Barents and Labrador Seas, due to the notably high skill in these regions. Before computing correlation values, both the SIE and ocean temperature time series are linearly detrended. The correlations are plotted for the upper 250 m of the ocean, which is roughly the depth of the Barents Sea shelf region. The Labrador Sea is substantially deeper, but we focus on this upper ocean region where the temperature correlations are strongest. We perform the analysis for regional-mean ocean temperatures because temperature anomalies are quite coherent over these regions (typical correlations between regional-mean values and spatial-grid point values are between 0.6 and 0.9). Using regional-mean temperatures allows us to move from four dimensions (latitude, longitude, depth, and lead time) to two dimensions (depth and lead time), greatly simplifying the analysis.

Physically, one expects upper ocean temperatures and regional SIE to negatively covary, since colder temperatures lead to more extensive sea ice, and vice versa. Indeed, we find clear negative correlations between observed winter Barents and Labrador SIE and the upper ocean temperatures used to initialize the forecasts. This indicates that the data assimilation system is able to capture interannual fluctuations in surface and subsurface ocean temperatures in these regions. While the correlations are negative in both regions, their spatial structures are distinct. In the Labrador Sea, the strongest correlations are located within the mixed layer and become surface intensified when the mixed layer shoals over the summer months. In contrast, the Barents Sea correlations are strongest beneath the mixed layer for summer initialization months and regain a surface signature for leads corresponding to initialization month May. This correlation structure closely resembles the mechanism for midlatitude SST reemergence [Alexander and Deser, 1995; Alexander *et al.*, 1999], in which early-spring SST anomalies are stored beneath the summer mixed layer and reemerge to the surface when the mixed layer deepens the subsequent fall/winter. By this mechanism, summer subsurface ocean temperature anomalies have the potential to impact sea ice growth rates the following fall/winter.

The correlation strengths in different target months reflect aspects of the SIE forecast skill shown in Figure 2. In particular, the Barents Sea ocean correlations are weaker for target month March, consistent with the drop in skill in this month. Similarly, the Labrador Sea skill increases in March, consistent with the stronger temperature correlations at leads 8 and 9 in this month. Correlations between SIE and temperature ICs are generally lower in the Bering Sea and Sea of Okhotsk (see Figure S5), which is consistent with the lower prediction skill in these regions.

The robust negative correlations in Figure 3 indicate that the winter SIE forecast skill in the Barents and Labrador Seas is partially attributable to accurate initialization of upper ocean temperatures. Due to imperfect observations and model biases, the ocean ICs produced by the assimilation system have errors relative to

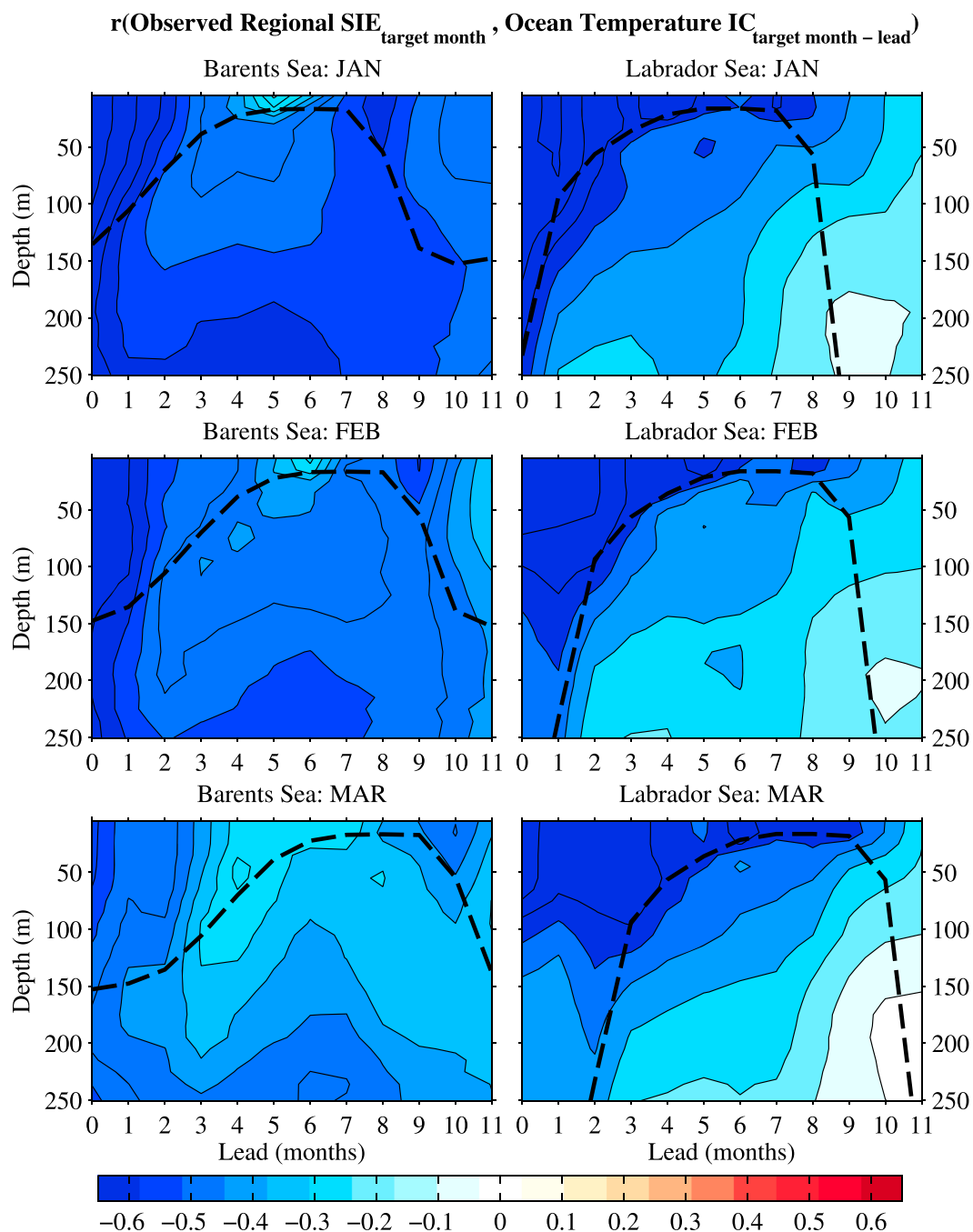


Figure 3. Correlation between observed regional SIE and regional-mean ocean temperature ICs in earlier months. Correlations are plotted as a function of ocean depth and forecast lead time for the Barents and Labrador Seas and target months of January–March. The linear trend is removed from both time series before the correlation is computed. The regional-mean mixed-layer depth climatology is plotted as dashed lines. Correlation values satisfying $|r| > 0.34$ are statistically significant at the 95% level.

the true observed ocean state. Therefore, improving ocean initialization may be a promising route to improving winter SIE prediction skill. Indeed, the correlations between ocean temperature ICs and model-predicted SIE (See Figure S6) are substantially higher than the correlations with observed SIE reported in Figure 3. The difference between the model-predicted and observed correlation values represents the potential skill improvements achievable via improved ocean initialization (see Figure S7). The primary difference in these correlations is located beneath the summer mixed layer, suggesting a future need for improved subsurface

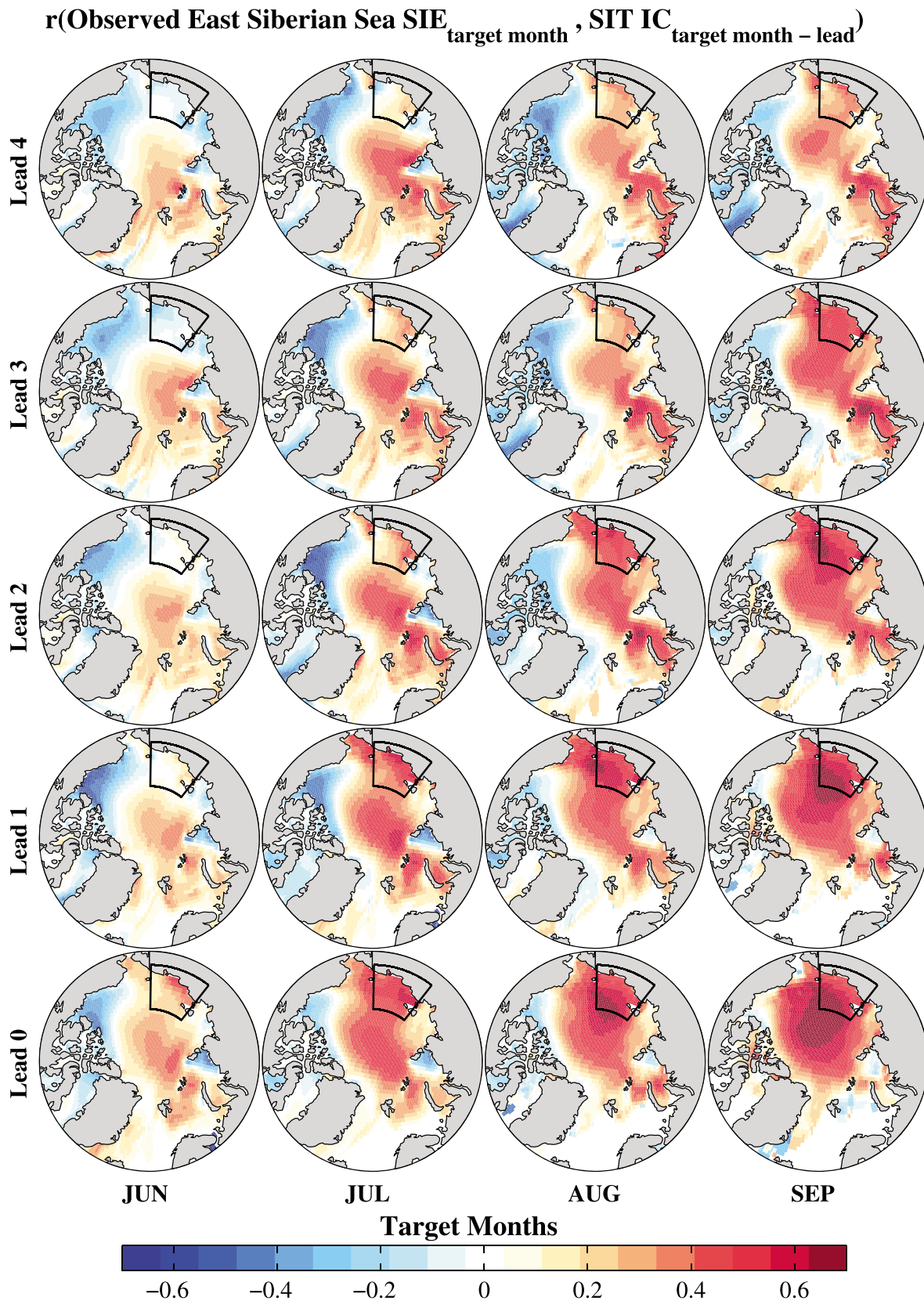


Figure 4. Correlations between observed East Siberian (boxed area) SIE and SIT ICs for different target months and forecast lead times. The linear trend is removed from both time series before the correlation is computed.

ocean observations. Also, we find that the correlations with model-predicted SIE have less dependence on the mixed-layer depth than the correlations with observed SIE (compare Figure S6 to Figure 3). In particular, the Barents Sea correlations have larger values within and near the mixed layer, whereas the Labrador Sea displays larger values below the mixed layer. This suggests that the correlation structures in Figure 3 do not necessarily reflect fundamental mechanisms of ice-ocean covariability of this model but instead may be partly associated with assimilation errors and/or model biases.

3.3. Sources of Summer Regional Skill: SIT Initialization

Next, we consider the sources of summer SIE prediction skill in the FLOR forecast system. Earlier work has shown that SIT is an important source of predictability for summer SIE on seasonal timescales [Holland *et al.*, 2011; Blanchard-Wrigglesworth *et al.*, 2011b; Chevallier and Salas y Méria, 2012; Lindsay *et al.*, 2012; Day *et al.*, 2014b; Germe *et al.*, 2014; Collow *et al.*, 2015; Guemas *et al.*, 2016; Bushuk *et al.*, 2017]. The ECDA system does not directly assimilate SIT data; however, it may implicitly capture interannual variations in SIT via its assimilation of atmospheric reanalysis data, which provides both thermodynamic and dynamic constraints on SIT. Lacking a long-term observational record of SIT, we compare ECDA SIT with the Pan-Arctic Ice Ocean Model and Assimilation System (PIOMAS) [Zhang and Rothrock, 2003], which is an ice-ocean reanalysis that agrees quite well with available satellite and in situ SIT observations [Schweiger *et al.*, 2011]. ECDA is biased thin relative to PIOMAS by 0.5–1 m but captures similar interannual variability in sea ice volume for all months of the year, with correlations ranging from 0.92 to 0.95 for total anomalies and 0.63–0.76 for detrended anomalies. Here we examine the relationship between summer regional SIE and earlier SIT ICs, focusing on the East Siberian, Laptev, Beaufort, and Chukchi Seas.

In Figure 4, we plot correlations between observed East Siberian Sea SIE and spatial-grid point values of SIT ICs in earlier months. Correlations are plotted for target months of June–September and lead times of 0–4 months. The linear trend is removed from both time series before the correlation is computed. We find that the local East Siberian SIE-SIT correlations are generally positive, consistent with the physical expectation that thicker initial sea ice should lead to more extensive summer sea ice, and vice versa. Moreover, we find that the SIE-SIT correlations have a diagonal structure that closely resembles the East Siberian ACC structure in Figure 2. This diagonal structure implies that the SIT initialization month is crucially important in determining East Siberian SIE skill. In particular, the East Siberian SIE-SIT correlation values are similar for July lead-0, August lead-1, and September lead-2, which each correspond to July-initialized forecasts. Similarly, there is a correspondence between July lead-1, August lead-2, and September lead-3 (June initialization) and July lead-2, August lead-3, and September lead-4 (May initialization). These SIE-SIT correlations suggest that the summer SIE skill in the East Siberian Sea is partially attributable to accurate initialization of local SIT anomalies. Note that the SIE-SIT correlations using model-predicted SIE are slightly stronger and also display a May prediction skill barrier (see Figure S8). This suggests that the May barrier is primarily related to the inherent predictability of East Siberian SIE, rather than resulting from SIT initialization errors.

SIT initialization also provides an important source of summer prediction skill in other Arctic regions with high summer SIE variability. Similar to the East Siberian Sea, we find that the SIE-SIT correlations in the Chukchi, Beaufort, and Laptev Seas (see Figures S9–S11, respectively) are consistent with the SIE prediction skill in these regions. The Chukchi Sea has SIE prediction skill up to leads of 4 months for target months June and July and lower skill for August and September (see Figure 2). The Chukchi region displays strong SIE-SIT correlations for leads 0–4 in June and July, and correspondingly lower correlations in August and September (see Figure S9). The Beaufort and Laptev Seas have similar prediction skill barriers to the East Siberian Sea (see the diagonal ACC structures in Figure 2). The SIE-SIT correlations for these regions display a diagonal structure consistent with these skill barriers (see Figures S10 and S11). These results demonstrate the importance of SIT ICs for summer SIE prediction and suggest that direct assimilation of thickness observations could potentially improve summer prediction skill.

4. Conclusions

This study has examined the seasonal prediction skill for Arctic regional SIE within the GFDL-FLOR dynamical forecast system. We have found that prediction skill for detrended regional SIE generally exceeds that of an anomaly persistence forecast. Prediction skill is notably high in the North Atlantic sector. Winter/spring Labrador SIE predictions are skillful at 7–11 month lead times, and predictions of winter SIE in the Barents and GIN Seas are skillful at 5–9 month lead times. Forecast skill is lower in the North Pacific sector, partially due

to the lower inherent persistence of regional SIE anomalies compared with their North Atlantic counterparts. Summer SIE forecasts are skillful at 1–4 month lead times in the East Siberian, Laptev, and Beaufort Seas and exhibit prediction skill barriers in which skill drops off sharply in particular initialization months (May, May, and June, respectively).

We have found that the initial conditions of the GFDL-FLOR prediction system provide a crucial source of prediction skill for both winter and summer regional SIE. In particular, the high prediction skill for winter SIE in the Labrador and Barents Seas is partially attributable to the accurate initialization and persistence of surface and subsurface ocean temperature anomalies. Similarly, the summer SIE prediction skill in the East Siberian, Laptev, Beaufort, and Chukchi Seas is partially attributable to the accurate initialization and persistence of SIT anomalies.

This study has provided an overview of regional Arctic SIE prediction skill and highlighted some key physical mechanisms underlying this skill. These results demonstrate the key role of subsurface ocean and SIT observations in predictions of regional SIE, emphasizing the need to both maintain and improve existing Arctic observing systems. In addition to higher-quality observations, the route to improved regional predictions depends crucially on reducing model biases, optimizing coupled data assimilation techniques, and understanding the detailed physical mechanisms that impact regional SIE. The results of this study motivate future work in regional sea ice prediction using this multifaceted approach.

Acknowledgments

We thank Charlie Stock and Desiree Tomassi for stimulating discussions and Dawei Li and Desiree Tomassi for comments on a preliminary version of this manuscript. This study was supported by NOAA's Climate Program Office, Climate Variability and Predictability Program (award GC15-504). The FLOR predictions analyzed in this work are available through the North American Multi-Model Ensemble (NMME) Phase-II data (<http://www.cpc.ncep.noaa.gov/products/NMME/data.html>). The NASA team sea ice concentration observations used in this study are available from the National Snow and Ice Data Center website (<http://nsidc.org/data/NSIDC-0051/versions/1>).

References

- Alexander, M. A., and C. Deser (1995), A mechanism for the recurrence of wintertime midlatitude SST anomalies, *J. Phys. Oceanogr.*, *25*(1), 122–137.
- Alexander, M. A., C. Deser, and M. S. Timlin (1999), The reemergence of SST anomalies in the North Pacific Ocean, *J. Clim.*, *12*, 2419–2433.
- Bauer, P., A. Thorpe, and G. Brunet (2015), The quiet revolution of numerical weather prediction, *Nature*, *525*(7567), 47–55.
- Bitz, C., M. Holland, A. Weaver, and M. Eby (2001), Simulating the ice-thickness distribution in a coupled climate model, *J. Geophys. Res.*, *106*(C2), 2441–2463.
- Blanchard-Wrigglesworth, E., C. Bitz, and M. Holland (2011a), Influence of initial conditions and climate forcing on predicting Arctic sea ice, *Geophys. Res. Lett.*, *38*, L18503, doi:10.1029/2011GL048807.
- Blanchard-Wrigglesworth, E., K. C. Armour, C. M. Bitz, and E. DeWeaver (2011b), Persistence and inherent predictability of Arctic sea ice in a GCM ensemble and observations, *J. Clim.*, *24*, 231–250.
- Blanchard-Wrigglesworth, E., R. Cullather, W. Wang, J. Zhang, and C. Bitz (2015), Model forecast skill and sensitivity to initial conditions in the seasonal Sea Ice Outlook, *Geophys. Res. Lett.*, *42*, 8042–8048, doi:10.1002/2015GL065860.
- Bretherton, C. S., M. Widmann, V. P. Dymnikov, J. M. Wallace, and I. Bladé (1999), The effective number of spatial degrees of freedom of a time-varying field, *J. Clim.*, *12*(7), 1990–2009.
- Bushuk, M., and D. Giannakis (2015), Sea-ice reemergence in a model hierarchy, *Geophys. Res. Lett.*, *42*, 5337–5345, doi:10.1002/2015GL063972.
- Bushuk, M., and D. Giannakis (2017), The seasonality and interannual variability of Arctic sea-ice reemergence, *J. Clim.*, doi:10.1175/JCLI-D-16-0549.1, in press.
- Bushuk, M., D. Giannakis, and A. J. Majda (2014), Reemergence mechanisms for North Pacific sea ice revealed through nonlinear Laplacian spectral analysis, *J. Clim.*, *27*, 6265–6287.
- Bushuk, M., D. Giannakis, and A. J. Majda (2015), Arctic sea-ice reemergence: The role of large-scale oceanic and atmospheric variability, *J. Clim.*, *28*, 5477–5509.
- Bushuk, M., R. Msadek, M. Winton, G. Vecchi, R. Gudgel, A. Rosati, and X. Yang (2017), Summer enhancement of Arctic sea-ice volume anomalies in the September-ice zone, *J. Clim.*, *30*, 2341–2362.
- Cavalieri, D. J., and C. L. Parkinson (2012), Arctic sea ice variability and trends, 1979–2010, *Cryosphere*, *6*(4), 881–889, doi:10.5194/tc-6-881-2012.
- Cavalieri, D. J., C. L. Parkinson, P. Gloersen, and H. J. Zwally (1996), *Sea ice concentrations from Nimbus-7 SMMR and DMSP SSM/I-SSMIS Passive Microwave Data, Version 1*, NASA DAAC at the Natl. Snow and Ice Data Cent., Boulder, Colo., doi:10.5067/8GQ8LZQVL0VL.
- Cheng, W., E. Blanchard-Wrigglesworth, C. M. Bitz, C. Ladd, and P. J. Stabeno (2016), Diagnostic sea ice predictability in the pan-Arctic and US Arctic regional seas, *Geophys. Res. Lett.*, *43*, 11,688–11,696, doi:10.1002/2016GL070735.
- Chevallier, M., and D. Salas y Mélia (2012), The role of sea ice thickness distribution in the Arctic sea ice potential predictability: A diagnostic approach with a coupled GCM, *J. Clim.*, *25*(8), 3025–3038.
- Chevallier, M., D. Salas y Mélia, A. Voldoire, M. Déqué, and G. Garric (2013), Seasonal forecasts of the pan-Arctic sea ice extent using a GCM-based seasonal prediction system, *J. Clim.*, *26*(16), 6092–6104.
- Collow, T. W., W. Wang, A. Kumar, and J. Zhang (2015), Improving Arctic sea ice prediction using PIOMAS initial sea ice thickness in a coupled ocean-atmosphere model, *Mon. Weather Rev.*, *143*(11), 4618–4630.
- Day, J., S. Tietsche, and E. Hawkins (2014a), Pan-Arctic and regional sea ice predictability: Initialization month dependence, *J. Clim.*, *27*(12), 4371–4390.
- Day, J., E. Hawkins, and S. Tietsche (2014b), Will Arctic sea ice thickness initialization improve seasonal forecast skill?, *Geophys. Res. Lett.*, *41*, 7566–7575, doi:10.1002/2014GL061694.
- Delworth, T. L., et al. (2006), Gfdl's CM2 global coupled climate models. Part I: Formulation and simulation characteristics, *J. Clim.*, *19*(5), 643–674.
- Ford, J. D., and B. Smit (2004), A framework for assessing the vulnerability of communities in the Canadian Arctic to risks associated with climate change, *Arctic*, *57*, 389–400.
- Germe, A., M. Chevallier, D. Salas y Mélia, E. Sanchez-Gomez, and C. Cassou (2014), Interannual predictability of Arctic sea ice in a global climate model: Regional contrasts and temporal evolution, *Clim. Dyn.*, *43*(9-10), 2519–2538.

- Guemas, V., M. Chevallier, M. Déqué, O. Bellprat, and F. Doblas-Reyes (2016), Impact of sea ice initialisation on sea ice and atmosphere prediction skill on seasonal timescales, *Geophys. Res. Lett.*, *43*(8), 3889–3896.
- Holland, M. M., D. A. Bailey, and S. Vavrus (2011), Inherent sea ice predictability in the rapidly changing Arctic environment of the Community Climate System Model, version 3, *Clim. Dyn.*, *36*(7–8), 1239–1253.
- Hunke, E., and J. Dukowicz (1997), An elastic-viscous-plastic model for sea ice dynamics, *J. Phys. Oceanogr.*, *27*(9), 1849–1867.
- Jia, L., et al. (2015), Improved seasonal prediction of temperature and precipitation over land in a high-resolution GFDL climate model, *J. Clim.*, *28*(5), 2044–2062.
- Jung, T., et al. (2016), Advancing polar prediction capabilities on daily to seasonal time scales, *Bull. Am. Meteorol. Soc.*, *97*, 1631–1647, doi:10.1175/BAMS-D-14-00246.1.
- Koenig, T., and U. Mikolajewicz (2009), Seasonal to interannual climate predictability in mid and high northern latitudes in a global coupled model, *Clim. Dyn.*, *32*(6), 783–798.
- Krikken, F., M. Schmeits, W. Vlot, V. Guemas, and W. Hazeleger (2016), Skill improvement of dynamical seasonal Arctic sea ice forecasts, *Geophys. Res. Lett.*, *43*, 5124–5132, doi:10.1002/2016GL068462.
- Kwok, R., and D. Rothrock (2009), Decline in Arctic sea ice thickness from submarine and ICESat records: 1958–2008, *Geophys. Res. Lett.*, *36*, L15501, doi:10.1029/2009GL039035.
- Laliberté, F., S. Howell, and P. Kushner (2016), Regional variability of a projected sea ice-free Arctic during the summer months, *Geophys. Res. Lett.*, *43*, 256–263, doi:10.1002/2015GL066855.
- Levitus, S., et al. (2013), The world ocean database, *Data Sci. J.*, *12*, WDS229–WDS234.
- Lindsay, R., J. Zhang, A. Schweiger, and M. Steele (2008), Seasonal predictions of ice extent in the Arctic Ocean, *J. Geophys. Res.*, *113*, C02023, doi:10.1029/2007JC004259.
- Lindsay, R., C. Haas, S. Hendricks, P. Hunkeler, N. Kurtz, J. Paden, B. Panzer, J. Sonntag, J. Yungel, and J. Zhang (2012), Seasonal forecasts of Arctic sea ice initialized with observations of ice thickness, *Geophys. Res. Lett.*, *39*, L21502, doi:10.1029/2012GL053576.
- Maslanik, J., J. Stroeve, C. Fowler, and W. Emery (2011), Distribution and trends in Arctic sea ice age through spring 2011, *Geophys. Res. Lett.*, *38*, L13502, doi:10.1029/2011GL047735.
- Melia, N., K. Haines, and E. Hawkins (2016), Sea ice decline and 21st century trans-Arctic shipping routes, *Geophys. Res. Lett.*, *43*, 9720–9728, doi:10.1002/2016GL069315.
- Merryfield, W., W.-S. Lee, W. Wang, M. Chen, and A. Kumar (2013), Multi-system seasonal predictions of Arctic sea ice, *Geophys. Res. Lett.*, *40*, 1551–1556, doi:10.1002/grl.50317.
- Msadek, R., G. Vecchi, M. Winton, and R. Gudgel (2014), Importance of initial conditions in seasonal predictions of Arctic sea ice extent, *Geophys. Res. Lett.*, *41*, 5208–5215, doi:10.1002/2014GL060799.
- Murphy, A. H. (1988), Skill scores based on the mean square error and their relationships to the correlation coefficient, *Mon. Weather Rev.*, *116*(12), 2417–2424.
- Perovich, D. K., and C. Polashenski (2012), Albedo evolution of seasonal Arctic sea ice, *Geophys. Res. Lett.*, *39*, L08501, doi:10.1029/2012GL051432.
- Peterson, K. A., A. Arribas, H. Hewitt, A. Keen, D. Lea, and A. McLaren (2015), Assessing the forecast skill of Arctic sea ice extent in the GloSea4 seasonal prediction system, *Clim. Dyn.*, *44*(1–2), 147–162.
- Petty, A. A., D. Schröder, J. Stroeve, T. Markus, J. Miller, N. Kurtz, D. Feltham, and D. Flocco (2017), Skillful spring forecasts of September Arctic sea ice extent using passive microwave sea ice observations, *Earth's Future*, *5*(2), 254–263.
- Pizzolato, L., S. E. Howell, J. Dawson, F. Laliberté, and L. Copland (2016), The influence of declining sea ice on shipping activity in the Canadian Arctic, *Geophys. Res. Lett.*, *43*, 12,146–12,154, doi:10.1002/2016GL071489.
- Regehr, E. V., N. J. Lunn, S. C. Amstrup, and I. Stirling (2007), Effects of earlier sea ice breakup on survival and population size of polar bears in western Hudson Bay, *J. Wildlife Manage.*, *71*(8), 2673–2683.
- Rigor, I. G., and J. M. Wallace (2004), Variations in the age of Arctic sea-ice and summer sea-ice extent, *Geophys. Res. Lett.*, *31*, L09401, doi:10.1029/2004GL019492.
- Roemmich, D., S. Riser, R. Davis, and Y. Desaubies (2004), Autonomous profiling floats: Workhorse for broad-scale ocean observations, *Mar. Technol. Soc. J.*, *38*(2), 21–29.
- Rothrock, D. A., Y. Yu, and G. A. Maykut (1999), Thinning of the Arctic sea-ice cover, *Geophys. Res. Lett.*, *26*(23), 3469–3472.
- Schröder, D., D. L. Feltham, D. Flocco, and M. Tsamados (2014), September Arctic sea-ice minimum predicted by spring melt-pond fraction, *Nat. Clim. Change*, *4*, 353–357.
- Schweiger, A., R. Lindsay, J. Zhang, M. Steele, H. Stern, and R. Kwok (2011), Uncertainty in modeled Arctic sea ice volume, *J. Geophys. Res.*, *116*, C00D06, doi:10.1029/2011JC007084.
- Serreze, M. C., M. M. Holland, and J. Stroeve (2007), Perspectives on the Arctic's shrinking sea-ice cover, *Science*, *315*(5818), 1533–1536, doi:10.1126/science.1139426.
- Sigmond, M., J. Fyfe, G. Flato, V. Kharin, and W. Merryfield (2013), Seasonal forecast skill of Arctic sea ice area in a dynamical forecast system, *Geophys. Res. Lett.*, *40*, 529–534, doi:10.1002/grl.50129.
- Sigmond, M., M. Reader, G. Flato, W. Merryfield, and A. Tivy (2016), Skillful seasonal forecasts of Arctic sea ice retreat and advance dates in a dynamical forecast system, *Geophys. Res. Lett.*, *43*, 12,457–12,465, doi:10.1002/2016GL071396.
- Smith, L. C., and S. R. Stephenson (2013), New Trans-Arctic shipping routes navigable by midcentury, *Proc. Natl. Acad. Sci.*, *110*(13), E1191–E1195.
- Stock, C. A., et al. (2015), Seasonal sea surface temperature anomaly prediction for coastal ecosystems, *Prog. Oceanogr.*, *137*, 219–236.
- Stroeve, J., T. Markus, L. Boisvert, J. Miller, and A. Barrett (2014a), Changes in Arctic melt season and implications for sea ice loss, *Geophys. Res. Lett.*, *41*, 1216–1225, doi:10.1002/2013GL058951.
- Stroeve, J., L. C. Hamilton, C. M. Bitz, and E. Blanchard-Wrigglesworth (2014b), Predicting September sea ice: Ensemble skill of the SEARCH sea ice outlook 2008–2013, *Geophys. Res. Lett.*, *41*, 2411–2418, doi:10.1002/2014GL059388.
- Sun, C., et al. (2010), The Data Management System for the Global Temperature and Salinity Profile Programme, in *Proceedings of OceanObs'09: Sustained Ocean Observations and Information for Society*, vol. 2, edited by J. Hall, D. E. Harrison, and D. Stammer, ESA Publ. WPP-306, Venice, Italy, 21–25 Sept. 2009, doi:10.5270/OceanObs09.cwp.86.
- Tietsche, S., J. Day, V. Guemas, W. Hurlin, S. Keeley, D. Matei, R. Msadek, M. Collins, and E. Hawkins (2014), Seasonal to interannual Arctic sea ice predictability in current global climate models, *Geophys. Res. Lett.*, *41*, 1035–1043, doi:10.1002/2013GL058755.
- Van den Dool, H. (2006), *Empirical Methods in Short-Term Climate Prediction*, Oxford Univ. Press, Oxford, U. K.
- Vecchi, G. A., et al. (2014), On the seasonal forecasting of regional tropical cyclone activity, *J. Clim.*, *27*(21), 7994–8016.
- Wang, L., X. Yuan, M. Ting, and C. Li (2016), Predicting summer Arctic sea ice concentration intraseasonal variability using a vector autoregressive model*, *J. Clim.*, *29*(4), 1529–1543.

- Wang, W., M. Chen, and A. Kumar (2013), Seasonal prediction of Arctic sea ice extent from a coupled dynamical forecast system, *Mon. Weather Rev.*, *141*(4), 1375–1394.
- Winton, M. (2000), A reformulated three-layer sea ice model, *J. Atmos. Oceanic Technol.*, *17*(4), 525–531.
- Wyllie-Echeverria, T., and W. S. Wooster (1998), Year-to-year variations in Bering Sea ice cover and some consequences for fish distributions, *Fisheries Oceanogr.*, *7*(2), 159–170.
- Yeager, S. G., A. R. Karspeck, and G. Danabasoglu (2015), Predicted slowdown in the rate of Atlantic sea ice loss, *Geophys. Res. Lett.*, *42*, 10,704–10,713, doi:10.1002/2015GL065364.
- Yuan, X., D. Chen, C. Li, L. Wang, and W. Wang (2016), Arctic sea ice seasonal prediction by a linear Markov model, *J. Clim.*, *29*(22), 8151–8173.
- Zhang, J., and D. Rothrock (2003), Modeling global sea ice with a thickness and enthalpy distribution model in generalized curvilinear coordinates, *Mon. Weather Rev.*, *131*(5), 845–861.
- Zhang, S., M. Harrison, A. Rosati, and A. Wittenberg (2007), System design and evaluation of coupled ensemble data assimilation for global oceanic climate studies, *Mon. Weather Rev.*, *135*(10), 3541–3564.